Protection and Control of Modern Power Systems

ORIGINAL RESEARCH Open Access

Load shedding strategy coordinated with storage device and D-STATCOM to enhance the microgrid stability

Sheetal Chandak[1*], Pritam Bhowmik[1] and Pravat Kumar Rout[2]

Abstract

Recently microgrids have drawn a potential attraction by fulfilling the environmental demands and the increasing energy demands of the end-users. It is necessary to focus on various protection and control aspects of a microgrid. During the transition between the grid-following and grid-forming modes, the voltage and the frequency instability due to the power mismatch condition becomes the major point of concern. Therefore, the paper executes a frequency-active power and voltage-reactive power drooping control strategy for the precise power-sharing among the distributed power generators. Furthermore, to handle the power deficit scenarios and to maintain the system stability, a system independent and priority-based adaptive three-stage load shedding strategy is proposed. The sensitivity of the strategy depends on the system inertia and is computed according to the varying absolute rate-of-change-of-frequency. The strategy incorporates the operation of battery storage system and distributed static compensator (D-STATCOM) in the microgrid, to provide a reliable power supply to the customers for a considerable time instead of a sudden load shedding. The effectiveness of the proposed strategies is investigated on a scaled-down modified IEEE 13-bus microgrid system on the podium of MATLAB 2015b through the time-domain simulation.

Keywords: Microgrid, Power-sharing, Load shedding, High inertia distributed generators, Inertia-less distributed generators, Battery storage system, D-STATCOM

1 Introduction

The incorporation of renewable power sources with the power utilities has been a promising solution towards the uninterrupted eco-friendly power demand. As a consequence, the installation and integration of distributed generators (DG) with the utilities appear as a major source of developing the small and medium-size microgrids [1]. Since the DGs in the conventional microgrid are operationally similar, the effects of disturbance and the amount of power to be shared are equally distributed without overloading any particular DG in the microgrid. But the voltage and the frequency at the point of common coupling (PCC) between the microgrid and utility undergo high distortion [2]. However, with the increased research efforts, the microgrids successively integrate the very differently operating DG (i.e., synchronous machine and inverter-based power sources). This incorporation of high inertia synchronous machines in an inertia-less dominated microgrid environment supports the system to ride through during the transient [3].

At the occurrence of any disturbance in the operationally diversified DG integrated microgrid, the power-sharing challenge arises. The inertia-less inverter-based DG can instantly respond to the fluctuation and vary the voltage according to the power required. Conversely, the sudden changes in the power are not feasible for high inertia based DG (synchronous machine). Further, the issue turns out to be critical, when the power generation of the operating DG reduces significantly due to the climatic condition [4]. Thus, the conjunction of high inertia power sources with the inertia-less sources challenges the operational stability. In order to address these issues, power-sharing integrated load shedding strategy is executed to enhance the performance of the microgrid [5, 6]. A two-phase droop based frequency control and a load shedding

* Correspondence: sheetalchandak91@gmail.com
[1]Electrical Engineering Department, Siksha 'O' Anusandhan University, Bhubaneswar 751030, India
Full list of author information is available at the end of the article

strategy are analyzed in [5] to maintain the stability of an autonomous microgrid.

To attain a stable electric system, various researchers have proposed several under-frequency load shedding (UFLS) schemes [7–9]. The conventional UFLS technique employs the strategy of shedding a fixed amount of load according to the predefined frequency limits. This conventional strategy uses a trial and error approach to calculate the number and the amount of load to be shed in each step. The strategy possesses a major drawback of shedding either the excessive or insufficient load amount, to attain the system stability [10]. Thus to shed an exact amount of load from an appropriate location brings into the adaptive UFLS scheme. The adaptive load shedding strategy sheds the load by measuring the frequency derivatives [11]. As a result, the load is shed based on the power deficit in each step.

Extensive work has been done in the field of adaptive UFLS. A comparison among the conventional, semi adaptive and adaptive UFLS is presented in [12]. The adaptive load shedding scheme implements rate-of-change-of-frequency in [11–13] and disturbance magnitude in [14] to shed the load. Further to enhance the shedding strategy, [13, 15] use voltage dependency of the load to shed the loads. In [16, 17] the frequency deviation is monitored in accordance with the inertia constant and follows a pattern of response based event approach. A strategy proposed in [18] implements shedding at the location where the voltage reduction and the frequency deviation is maximum. Integer programming and genetic algorithm are executed in load shedding strategies by [19, 20]. Moreover, certain smart-grid load shedding strategies are introduced by [21, 22]. The strategies proposed till now need to be explored further to achieve efficient performance in a microgrid environment. The microgrid system with multiple numbers and multiple types of power sources, storage devices, and loads, challenges the calculation of exact values for the load shedding parameters. Furthermore, the slightest interruption in an isolated microgrid can affect system stability. A reactive power deficit during the autonomous mode of operation may lead the system towards voltage sag. Subsequently, the voltage sags vary the amount of power drawn by the load. As a result, delay in the measurements of frequency and its derivative may mislead the shedding strategy, because the estimated power shortage will be lesser than the actual deficit. Further, an additional drawback of this strategy is the non-linear relationship between the amount of load shed and the power deficit.

In order to further enhance the adaptive UFLS scheme in accordance with the transient stability, storage elements like ultracapacitor are incorporated to impart dynamic frequency support by [23]. Further to compensate for the frequency variations until the governor response comes into action, the superconducting storage devices are implemented by [24]. The super magnetic energy storage device to enhance transient stability while shedding the loads are also employed in [25]. However, the implementation of fast-responding storage devices cannot be imposed with the frequency limit and their energy recovery factor. Further, the presence of slow-responding storage devices in the microgrid is yet to be considered while designing the UFLS.

The energy storage system has been an indispensable part of the microgrid. The addition of a storage system is a smart way to curb the power fluctuations and counteract the power imbalances [26]. Besides that, the storage system plays a significant task in improving the system reliability and stability in a microgrid (comprising a major share of renewable sources). Its integration could set-back the cost of improving the transmission and distribution capacity to address the increasing power demand [27]. Thus, a battery energy storage (BES) device is integrated into the microgrid system to counteract the power deficits. The operation of BES is incorporated with the load shedding strategy to support the local loads from the instantaneous power cut-off during the unstable system operation.

However, the incorporation of the battery storage devices cannot always ensure a robust transient support system because these storage elements offer low power density with respect to their storage volume. Though these kinds of storage devices increase the relative inertia of the microgrid, but fail during the transient period. In other words, the microgrid lacks the required amount of inertia to withstand the transient fluctuations due to the system disturbances. Therefore, considerable attention has been drawn towards the integration of distributed static compensator (D-STATCOM) in the microgrids.

D-STATCOMs solely perform to improve the load balancing and power factor of a system [28]. The incorporation of D-STATCOMs in the distribution structure has drawn a significant interest because of its novel characteristic of compensating either PCC voltage or the line current [29]. Thus in this paper, the D-STATCOM performs to avoid the instantaneous conflict of power-sharing between the two different types of inertial DG by compensating the voltage. The paper also highlights that the D-STATCOM and the high inertia system can efficiently control the system stability for a few cycles until the load shedding is initialized.

The paper proposes a reliable load shedding strategy along with an efficient power-sharing among the different inertial DGs. In the hierarchical control of microgrids, the secondary control focuses on power-sharing and load shedding. The paper implements a self-tuned

proportional-integral strategy with a power-sharing approach. The scheme implements the inertial-less and high inertial DGs, battery storage system, and D-STATCOM to monitor the voltage and frequency of the microgrid. However, a major emphasis has been given to a system scenario, where the load demand is greater than the power generated. Thus to deal with this scenario, a system independent and priority-based adaptive three-stage load shedding strategy is proposed. The strategy consists of a three-stage load shedding along with the consideration of the energy storage system (ESS). The fast-responding D-STATCOM is considered to deal with the transient events and reactive power deficits and the slow responding battery energy storage systems are considered to prolong the system stability by a certain time span. Thus, the major highlights of the proposed work are as follows:

- A detailed analysis of a P-f and Q-V droop control strategy to attain an efficient power-sharing among the different inertial DGs.
- The paper proposes an independent and priority-based adaptive three-stage load shedding strategy.
- To enhance the system stability, the performance of the battery and D-STATCOM present in the microgrid is closely analyzed while executing the load shedding algorithm.

The manuscript is organized as follows: Section II introduces the test system undertaken. Section III describes the controller design for each power source incorporated in the microgrid. The proposed control method for power-sharing and load shedding is extensively described in Section IV. The test results of the proposed strategy are analyzed in Section V. A brief discussion and conclusion obtained from the result analysis are discussed in Section VI and Section VII respectively.

2 Microgrid structure

A balanced three-phase 13 bus microgrid system considered in this study is represented in Fig. 1. The scaled-down test system comprises an inertia-less photovoltaic (PV) micro-source (DG-1), a high inertia synchronous machine (DG-2) and some distributed controllable loads. The designed microgrid integrates a battery storage device and distribution static compensator. The designed storage system is a scalable system. They are designed such that their characteristics can be studied within a smaller time span. However, for real-time implementation, the system ratings can be varied.

The system parameters are presented in the Appendix. The microgrid covers a distance of 8200 ft. length. The designed microgrid is integrated with the utility via a 115 kV(delta)/25 kV(grounded wye) substation transformer. The Simulink platform of MATLAB 2015b is used to replicate and test the designed microgrid system.

3 Controllers of power sources

3.1 Micro-sources

The designed inertia-less inverter based photovoltaic system generates a maximum of 100 kW at 1000 W/m^2 solar irradiance. The maximum power point tracking (MPPT) uses the Incremental Conductance

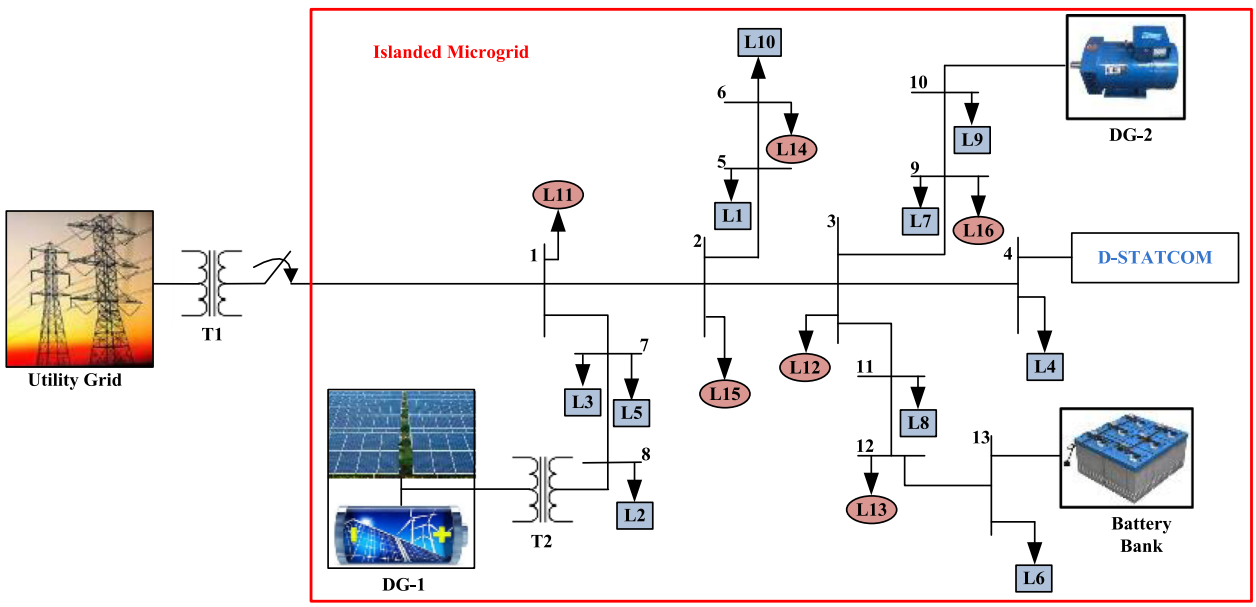

Fig. 1 System under study

method. The duty cycle controlled by the MPPT varies according to the voltage required to maximize the power extraction [30]. The DC-AC inverter converts the maximum extracted DC power to AC power using the control based on the dq reference frame. The control is designed such that it varies the DC link voltage according to the voltage variations at the PCC. The extracted power from the PV system is fed to the DC link [31]. Therefore, the V_{dc} controller in the inverter, controls the voltage variations by specifying the d-axis current ($I_{d_{ref}}$) values to balance the power flow in the DC link [32]. Since the system is considered to be operating at unity power factor, the reactive reference current ($I_{q_{ref}}$) is considered to be zero. Further, the control system implements the phase-locked loop to maintain the inverter voltage in phase with the grid voltage. The d-q axis currents when fed to the proportional-integral (PI) controllers, it helps in obtaining the reference voltages for the sinusoidal pulse width modulator (SPWM). The control design for the inertia-less inverter-based DG is shown in Fig. 2a.

The instantaneous voltage of a DG-1 connected to 13 bus test feeders can be written as in (1).

$$\frac{d}{dt} i_{DG-1} = \frac{-R_f}{L_f} i_{DG-1} + \frac{1}{L_f} [v_{DG-1} - v_{PCC}] \tag{1}$$

here, the i and v terms represent the instantaneous current and voltage respectively. R_f and L_f signify the resistance and the inductance of the filter respectively.

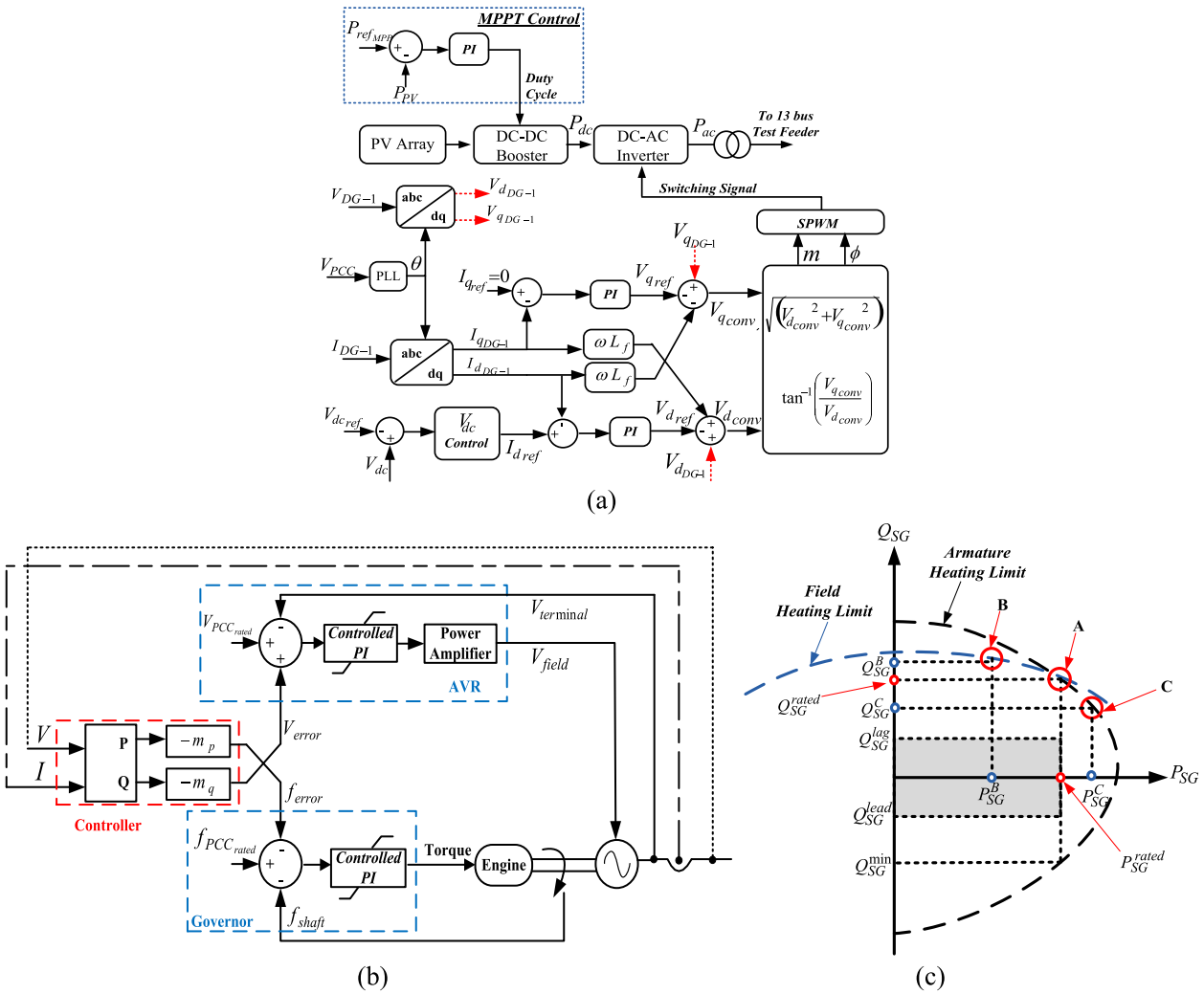

Fig. 2 Controller designed for DPG. **a** Inverter based distributed power generators, **b** Control of synchronous generators, **c** Synchronous generator capability curve

On using the Park's transformation on (1) to transform it into the rotating reference frame, the equation is reframed as:

$$\frac{d}{dt}\begin{bmatrix} i_{d_{DG-1}} \\ i_{q_{DG-1}} \end{bmatrix} = \begin{bmatrix} \frac{-R_f}{L_f} & 0 \\ 0 & \frac{-R_f}{L_f} \end{bmatrix} \begin{bmatrix} i_{d_{DG-1}} \\ i_{q_{DG-1}} \end{bmatrix} + \frac{1}{L_f}\begin{bmatrix} v_{dconv} \\ v_{qconv} \end{bmatrix} \tag{2}$$

where,

$$v_{dconv} = v_{d_{DG-1}} - v_{d_{PCC}} + \omega L_f i_{q_{DG-1}} \tag{3}$$
$$v_{qconv} = v_{q_{DG-1}} - v_{q_{PCC}} - \omega L_f i_{d_{DG-1}}$$

Using the terms v_{dconv} and v_{qconv}, the magnitude and the angle for the SPWM are generated. Hence, the inverter's switching pattern is signalled using (4).

$$\phi = \tan^{-1}\left(v_{qconv}/v_{dconv}\right) \tag{4}$$
$$m = \sqrt{v_{d_{conv}}^2 + v_{q_{conv}}^2}$$

The major advantages of using a current-control strategy can be stated as:

1) It provides protection against the over-current.
2) It reduces the contribution of fault currents by the unit.
3) It limits the converter output current during fault conditions.

On the other hand, the design of a high inertia synchronous system regulates the voltage and the frequency by a different approach. The frequency of the generator is regulated by adjusting the torque on the basis of speed error. Simultaneously the reference speed is adjusted according to the active power measured. Further, the automated voltage regulator (AVR) integral action regulates the voltage when the voltage reference error becomes zero [33]. The control strategy of the generator is presented in Fig. 2b.

The synchronous generator feeds both the active and the reactive power simultaneously up to certain limits of MVA rating according to the prime mover's capability. These limits can be obtained from the capability curve of the synchronous generator. The curve in Fig. 2c defines the inter-relation between the active and the reactive power to be generated by the generator. The shaded portion under the capability curve in Fig. 2c represents the required quantity of reactive power to be generated by the generator. Further, the point of intersection between the armature heating limits and field heating limits specifies the MW and MVAR rating of synchronous generators [34]. In Fig. 2c, it can be analyzed that intersecting point 'A' sets the generator active power as P_{SG}^{rated} and reactive power at Q_{SG}^{rated}. The reactive power can be fed until it reaches the heating limits (i.e., Q_{SG}^{rated}). However, if the reactive power to be fed is further increased to Q_{SG}^{B} at point B in Fig. 2c, it is delivered by reducing the active power generation as P_{SG}^{B} (where $P_{SG}^{B} < P_{SG}^{rated}$). The limits on the reactive power generation are set by either the armature heating limits as in point 'B' or by the field heating limits as in point 'C' [35].

3.2 D-STATCOM

D-STATCOM is a shunt connect voltage source converter (VSC) in the distributed power system. The integration of D-STATCOM in the power system is the most effective solution for reactive power compensation. A sudden change in reactive power demand or supply cannot be compensated by a synchronous machine, as fast as the voltage source converter [36]. It regulates the line voltage to control the leading or the lagging reactive power in the system with a response speed of 1-2 cycles [37]. Thus, the compensating device helps to regulate the voltage within its rated limit by efficient power management. In a grid-connected microgrid, the voltage fluctuations are majorly detected at the load end of the feeder. However, it is not possible to detect the voltage drop and the compensation point in an islanded microgrid. Therefore, the designed D-STATCOM is interconnected in the microgrid with the bus having critical loads. Figure 3 presents the schematic layout of the reactive power compensating D-STATCOM connected to the critical load.

The major role of D-STATCOM is to perform a conversion of input DC voltage to an output three-phase AC voltage. The instantaneous input and output power have to be balanced properly. Therefore, the input terminal of VSC is connected to a capacitor, which acts as a passive voltage source. On the other hand, the output of the VSC is connected to a coupling transformer, which acts as a passive current source.

The output current fed by the D-STATCOM can be expressed as in (5).

$$I_{stat} = \frac{V_{stat} - E}{X} \tag{5}$$

Here, V_{stat} and E represent the voltage at D-STAT COM and bus respectively, X signifies the system reactance and I_{stat} presents the current fed by the D-STAT COM. On using eq.(5), the reactive power compensated by the D-STATCOM can be stated as:

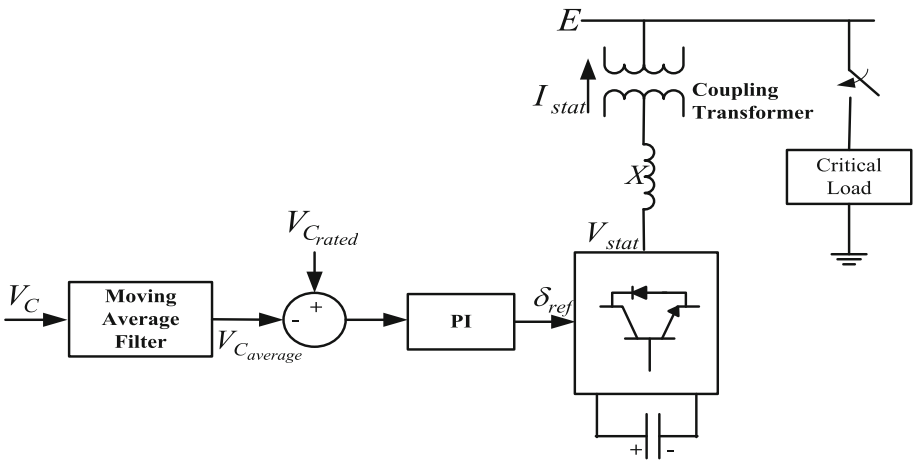

Fig. 3 Controller design for D-STATCOM

$$Q_{stat} = \frac{1-\left(\frac{E}{V_{stat}}\right)}{X} V_{stat}^2 \tag{6}$$

Analyzing (6), it can be clearly stated that the voltage fed by the D-STATCOM regulates the reactive power of the system [38]. The control over reactive power is attained by keeping the D-STATCOM voltage in phase with the system voltage. Moreover, these in phase voltages do not allow the charged capacitor to supply active power into the system. Further, at zero frequency of the DC capacitor, the reactive power of D-STATCOM is zero. Thus, it can be concluded that the DC capacitor does not play a role in reactive power generation. It proves that the VSC of D-STATCOM is capable of facilitating the free flow of reactive power among the three AC terminals [39]. The DC capacitor only enables the compensation for the instantaneous power mismatch in the system.

3.3 Storage device

The storage system considered in this study is the Lithium-Ion battery model acquired from the Matlab *SimPowerSystems* library. The battery parameters are set to support the P-f and Q-V control within the system. In-depth analysis regarding the storage devices presented in [40]. Due to the uncertain fluctuations in renewable power generation and load demands, lithium-ion batteries are highly preferable in microgrids. This is due to the fact that these batteries can be exploited up to their maximum capacity [41]. Therefore, to achieve a deep cycle operation, the lithium-ion batteries have been modelled with the proper selection of parameters.

The voltage of a completely charged Li-Ion battery (i.e., $E_{battery}$) can be expressed as:

$$E_{battery} = E_0 - K\frac{Q}{Q_{actual} - 0.1*Q} \cdot \left(i_{filtered}\right) - K\frac{Q}{Q - Q_{actual}} \cdot \left(Q_{actual}\right) + A\ \exp\left(-B.Q_{actual}\right) \tag{7}$$

The analytical battery model can be presented by (8) and (9) for charging and discharging respectively.

3.3.1 Charge

$$V_{battery} = E_0 - R_{\text{int}} \cdot I_{battery} - K\frac{Q}{Q_{actual} - 0.1*Q} \cdot \left(i_{filtered}\right) - K\frac{Q}{Q - Q_{actual}} \cdot \left(Q_{actual}\right) + A\ \exp\left(-B.Q_{actual}\right) \tag{8}$$

3.3.2 Discharge

$$V_{battery} = E_0 - R_{\text{int}} \cdot I_{battery} - K\frac{Q}{Q - Q_{actual}} \cdot \left(Q_{actual} + i_{filtered}\right) + A\ \exp\left(-B.Q_{actual}\right) \tag{9}$$

where, $V_{battery}$ and $I_{battery}$ represent the battery voltage and current respectively. K signifies the polarisation constant and R_{int} signifies the internal battery resistance. The battery capacity is represented by Q whereas the actual charge of the battery is presented by Q_{actual}. The constant voltage and the filtered current of the battery are stated as E_0 and $i_{filtered}$ respectively. To address the exponential zone of amplitude and time constant inverse, under the characteristic curve of the battery are termed as A and B respectively [42].

The assumption made for the undertaken battery system is that it can discharge up to State-of-Charge (SoC) being 30%. The battery parameters are set to reduce the rate of discharge after 50% of SoC is attained.

4 Proposed control method for microgrid

In order to attain a balanced voltage profile and a reduced system loss, efficient power-sharing is crucial. Power-sharing can be controlled either by implementing a communication-based centralized control strategy or by decentralized droop strategy. In recent times, communication strategies are avoided because of their economic limitations. Moreover, the interruptions and break-down in communication are few added up limitations to the communication-based control strategy. Hence, decentralized droop control strategies have drawn major attention. The droop control facilitates faster stability and an efficient power-sharing among the distributed generations in a microgrid.

The droop strategy can be explained using the basic circuit of two AC sources (i.e., $V_1 \angle \delta$ and $V_2 \angle 0$) connected by reactance (X) dominated impedance line. The power transfer between the two sources can be termed as:

$$P = \frac{V_1 V_2 Sin\delta}{X} \tag{10}$$

$$Q = \frac{V_1^2 - V_1 V_2 Cos\delta}{X} \tag{11}$$

It can be analyzed that the active power transferred is in proportion to δ, as the angle tends to be small during the normal operation of the system. The reactive power transferred also varies proportionally with the difference between the voltage magnitudes at the two ends [43]. Thus, the droop characteristics can be framed as in (12) and (13), and are graphically shown in Fig. 4.

$$\begin{aligned} &\omega = \omega_{\max} - m_p P \\ &\Rightarrow m_p = \frac{\omega_{\max} - \omega_{\min}}{P_{\max}} \end{aligned} \tag{12}$$

$$\begin{aligned} &V = V_o - n_q Q \\ &\Rightarrow n_q = \frac{V_{\max} - V_{\min}}{2Q_{\max}} \end{aligned} \tag{13}$$

Therefore, the control strategy of DGs present in an inductance-dominated microgrid implements active power-frequency (P-f) and reactive power-voltage (Q-V) droop control characteristics [44]. The strategy aims to maintain the voltage and the frequency of the microgrid within its limit, along with a precise power-sharing between the multiple power generators present in the microgrid.

In spite of an efficient power-sharing strategy, the microgrid may undergo an instability while experiencing an overloading condition. In an autonomous mode, the distributed power generators sacrifice their frequency and voltage to increase the power generation. This leads to a reduction in voltage and frequency, which may go beyond the specified threshold limits and cause a system blackout. A self-governing microgrid manages the power shortage either by increasing the power generation or by shedding the increased power demand. As a result, the system response due to the increased generation or reduced load demand is incorporated to restore the voltage and frequency stability. Thus, the paper proposes a load shedding strategy along with power-sharing.

A system independent and priority-based adaptive three-stage load shedding strategy is proposed. It deals with the power inequality in a microgrid after the occurrence of an islanding event. The rate-of-change-of-frequency is considered to compute the amount of load to be shed. At the beginning of the load shedding algorithm, it verifies the presence of a storage system. The stored battery power supports to prolong the load for a certain time. The first stage of the strategy controls the rapid frequency drop by shedding large loads. It also causes the system frequency to settle within the specified operational lower limit ($f \geq 59.3$).

As the grid-forming microgrid possesses minimum inertial stability, it becomes highly sensitive to the dynamic load demand. This sensitivity increases the system instability with the increment in the frequency deviation. Therefore, in the second and third stages of the proposed load shedding algorithm, it has been observed that the operating frequency tends to maintain the nominal frequency (60 Hz). Thus, to reach the predetermined operating value of the system frequency, the second stage of load shedding strategy triggers and sheds small load in iterative steps. Subsequently, the third stage of load shedding tends the difference between the operating

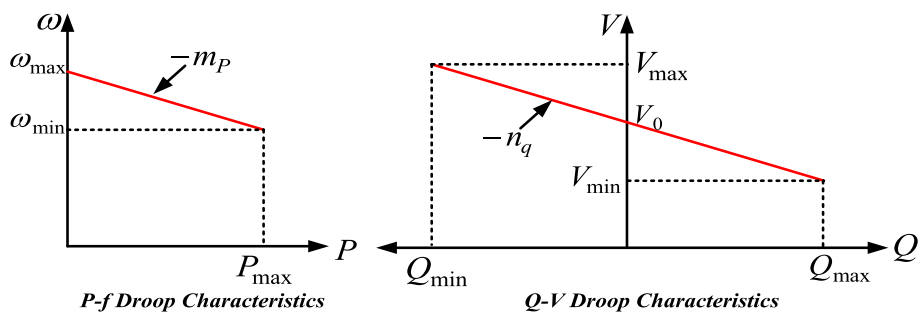

Fig. 4 Droop characteristics for power-sharing

frequency and the nominal frequency to approximately zero by shedding the very small loads. The algorithm for the proposed load shedding scheme is presented in Fig. 6 and each shedding stage is analyzed in the section as follows:

4.1 Proposed load shed amount

Stage-I, stage-II, and stage-III of the load shedding scheme shed the load by measuring the frequency, the rate-of-change-of-frequency and Δf respectively. However, the amount of shed load differs in each stage. The proposed scheme ensures an iterative shedding process and the sheddable loads from busses are decided using the strategy presented in [45]. The iteration continues until it satisfies the individual criterion. The scheme computes the shedding amount concerning the instantaneous rate of change of frequency measured. From Fig. 5 it can be observed that the rate-of-change-of-frequency varies significantly during the transition between the stages. The load to be shed during an iteration is computed using (14).

$$P_{Load-shed} = K*abs\left(\frac{df}{dt}\right) \tag{14}$$

where,

$$K = \frac{2*H_{equivalent}}{f_{rated}} \tag{15}$$

Here, $P_{Load-shed}$ is the amount of load shed in each iteration, and K denotes the shedding constant obtained from the swing equation of the system. $H_{equivalent}$ denotes the normalized inertia constant.

It can be observed from Fig. 5 that the rate-of-change-of-frequency at PCC is significantly high and it is a directly dependent factor of the power deficit. At the occurrence of an islanding instant, the significant difference in rate-of-change-of-frequency occurs due to the reduced moment of inertia of the grid-forming microgrid. As a result, the amount of load shed is directly proportional to the frequency derivative. Further, Fig. 5 illustrates that, with every step of load shed, the rate-of-change-of-frequency reduces with reducing power deficit and tends to attain approximately zero. Thus on realizing eq.(14), it can be analyzed that with the decrease of rate-of-change-of-frequency, the amount of load shed decreases. Therefore, this strategy of shedding the load amount in the proposed load shedding scheme presented in Fig. 6 helps to shed the proportional amount of load concerning the power deficit.

4.2 Battery and DSTATCOM performance simultaneously with the proposed load shedding strategy

The presence of a storage system in a microgrid adds to the advantages of the proposed load shedding strategy. It provides a certain amount of power to the extra loads by a certain period of time. The battery storage element supports during the islanded microgrid and compensates for the steady part of the power deficit. Conversely, the D-STATCOM compensates the system disturbances during the transients. The batteries supply a steady power at a specified nominal rate of discharge (RoD_1) till they reach 50% and at RoD_2 till they reach 30% of their state-of-charge (SoC). The SoC of a battery is a time-scaled factor with respect to the rate of power delivery. In other words, the instantaneous change in power supply does not change the SoC instantaneously. Therefore, considering the deep discharge limit of the battery, the power supplied by the battery is intentionally reduced to RoD_2 at a specified SoC condition of 50%. It can be observed from Fig. 6 that the algorithm clearly shows the operational performance of the storage device.

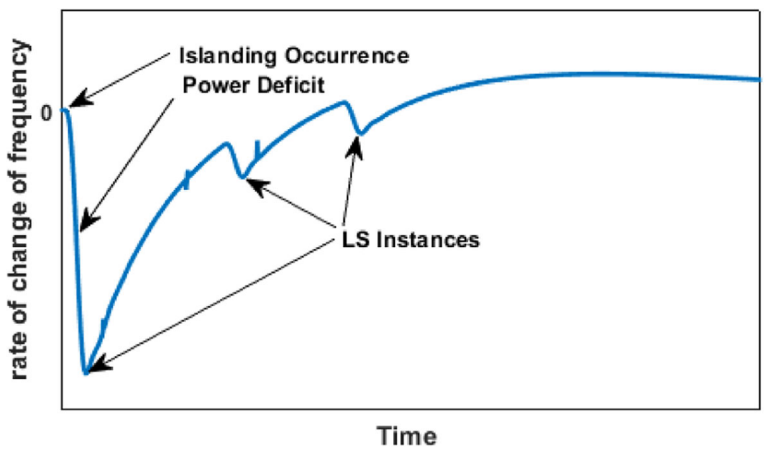

Fig. 5 Response of rate-of-change-of-frequency with respect to the power deficit

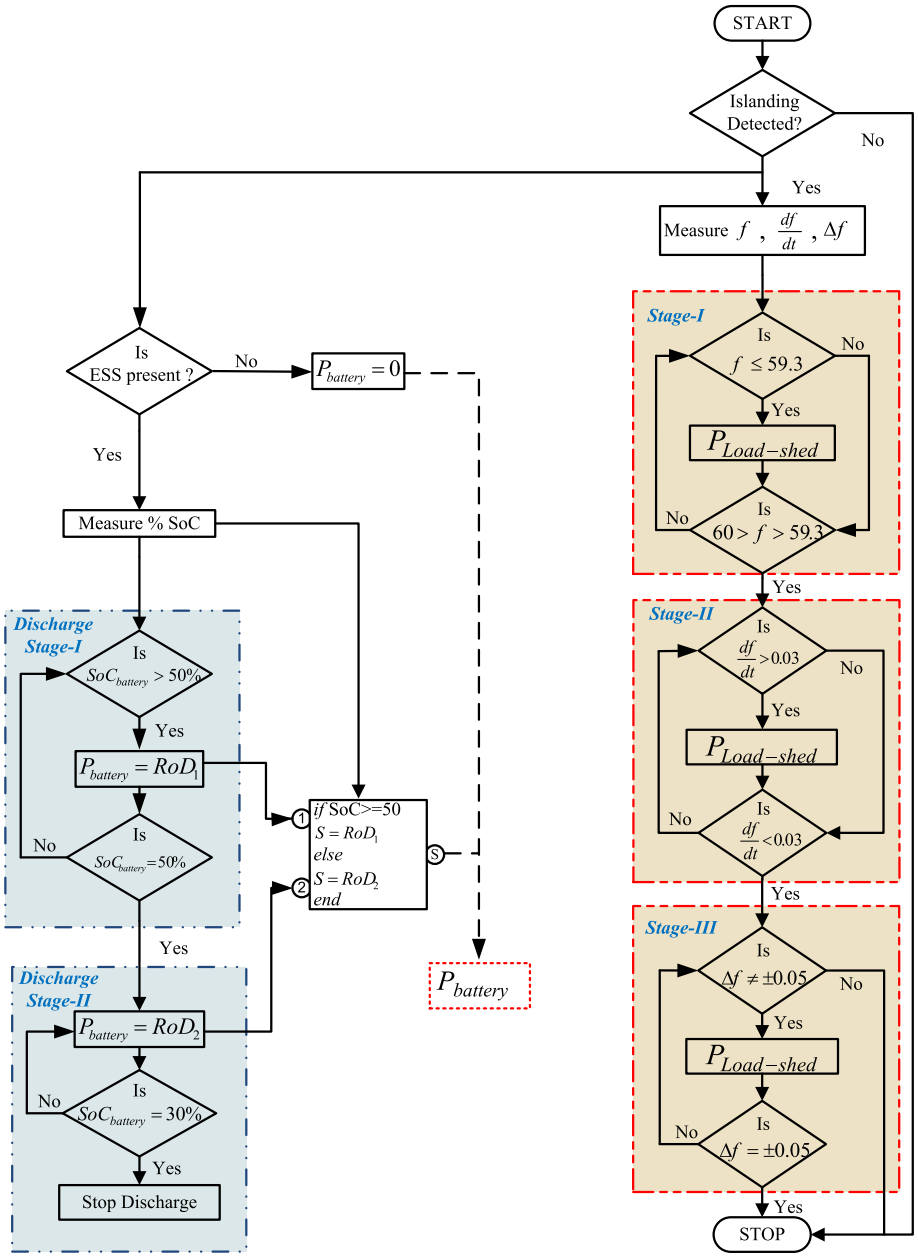

Fig. 6 Proposed load shedding algorithm

4.3 Stage-I of load shedding

The first stage of the proposed load shedding scheme functions with the objective to hold back the normal operating conditions of the microgrid after facing a severe power deficit. In Fig. 6, load shedding steps involved in each stage are highlighted. From the conventional strategy of power networks, it is observed that the rate of decrement of the frequency inversely depends on the cumulative short-circuit MVA of the entire integrated system [46]. However, in the microgrid the short-circuit MVA dramatically falls down due to the power electronic interfaces present in the system. Therefore, the microgrid fails to withstand the extra load demand. As a result, at the instant of islanding, system frequency drops down in proportion to the surplus load demand. The analyzed microgrid characteristic can be observed in Fig. 5. From Fig. 5 it can be clearly observed that the rate-of-change-of-frequency is proportional to the microgrid demand. So, to regain the rate-of-change-of-frequency, a large load is shed using eq.(14) in an iterative process. Thus, the load shedding starts when the system frequency goes beyond 59.3 Hz. The iterative process continues until the frequency regains to the given

threshold set value $f \geq 59.3$. The instant, when the microgrid reaches the set frequency limit for operational stability, the stage-II triggers.

4.4 Stage-II of load shedding

The loads in this stage are shed by considering the rate-of-change-of-frequency $(^{df}/_{dt})$. Smaller values of load shed in each step tends the frequency towards the operating nominal frequency of 60 Hz. The proposed algorithm in Fig. 6 illustrates that the iterative shedding process in this stage continues until the rate-of-change-of-frequency is less than 0.03.

4.5 Stage-III of load shedding

Now, as soon as the rate-of-change-of-frequency attains its 0.03 limit, the third stage of load shedding starts. In this stage, the Δf (i.e., difference between the operating frequency and the nominal frequency (60 Hz)) is calculated to shed small loads. The intention of this stage is to make $\Delta f = \pm 0.05$, by shedding small load iteratively. The stage-III of the load shedding strategy sheds the

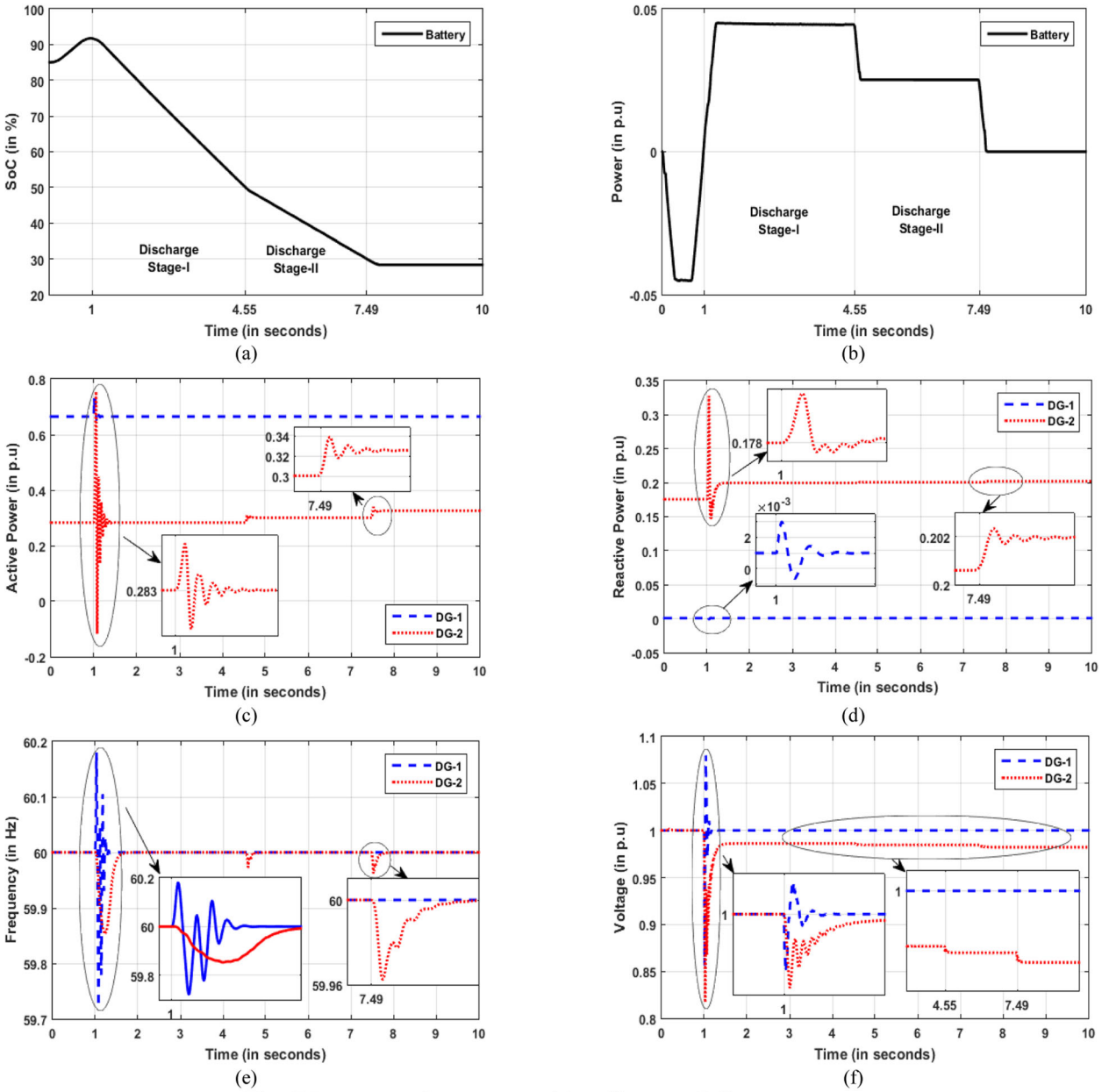

Fig. 7 Battery performance and its effects on DG parameters (**a**) Battery's state of charge, (**b**) Battery power, (**c**) Active power fed by the DGs, (**d**) Reactive power fed by the DGs, (**e**) Frequency variation in DGs, (**f**) Voltage variation in DGs

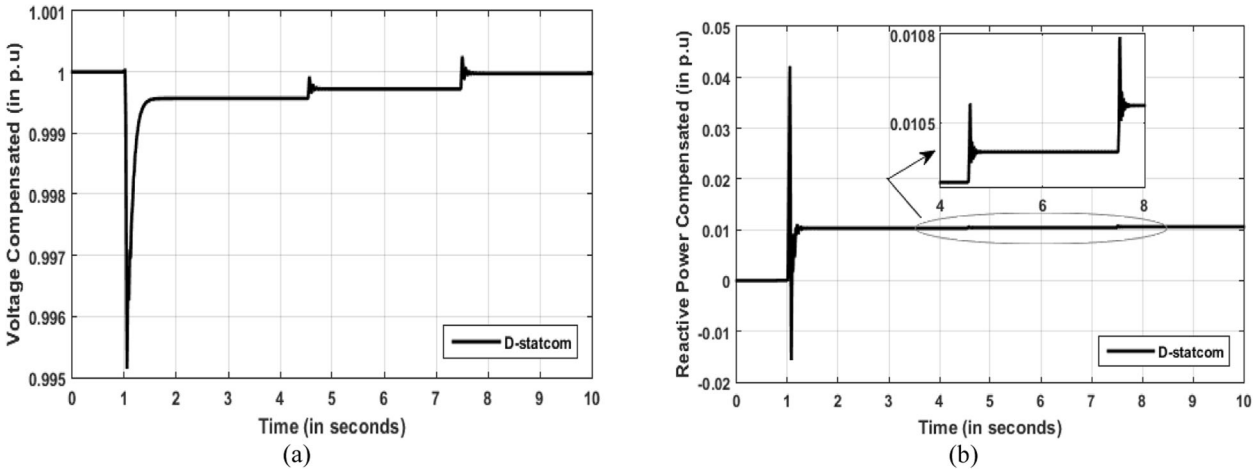

Fig. 8 D-STATCOM's performance (**a**) Voltage compensated, (**b**) Reactive power compensated

loads in a very small amount and makes the system stable. The stage reaches an end on achieving the Δf to be approximately zero.

The amount of load shed in each iteration and in each stage of the algorithm is based on the absolute rate-of-change-of-frequency of the microgrid. Hence, the shedding scheme is independent of the power generation. As a result, the climatic challenges or the operational challenges will not affect the load shedding strategy. Thus, the load shedding controls the microgrid to attain

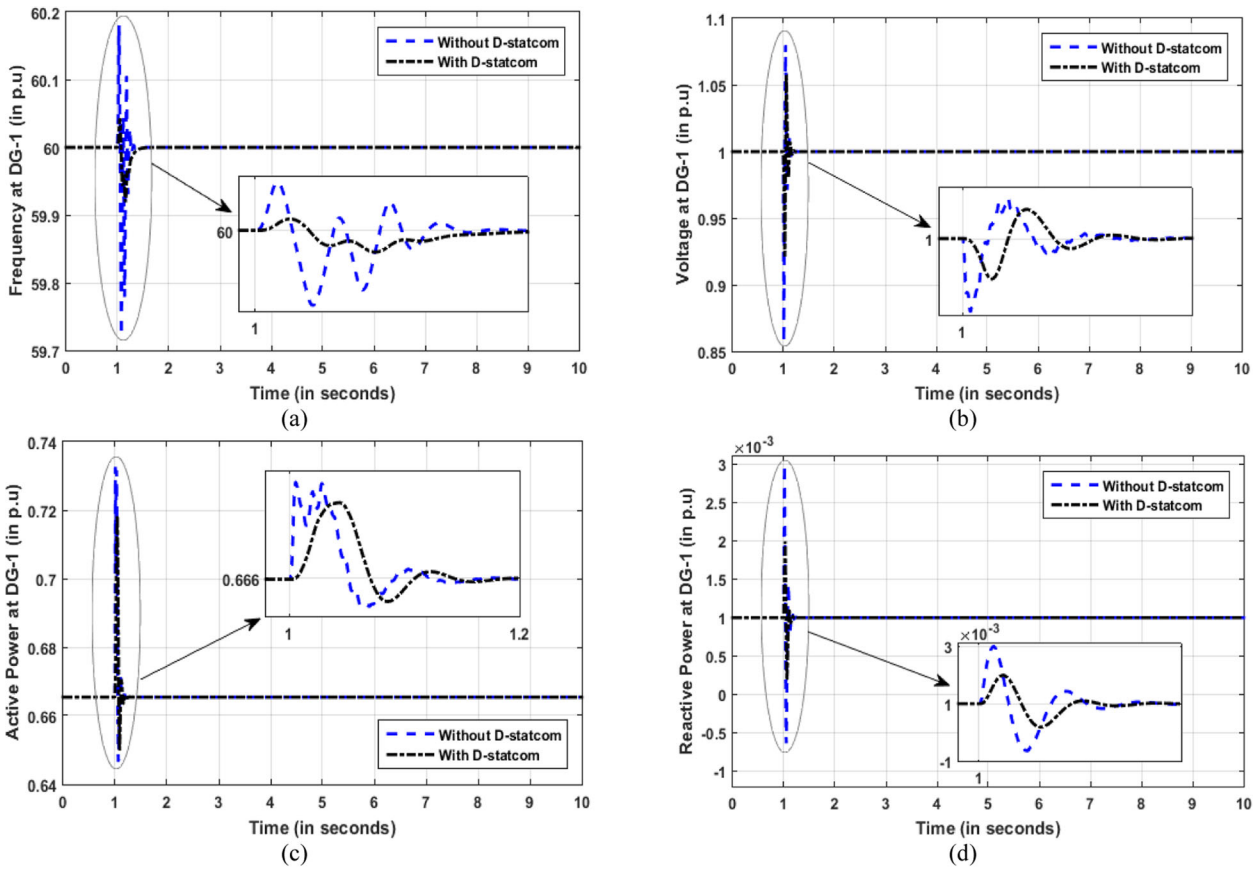

Fig. 9 Effects of D-STATCOM on the DG-1 parameters (**a**) Frequency, (**b**) Voltage, (**c**) Active power, (**d**) Reactive power

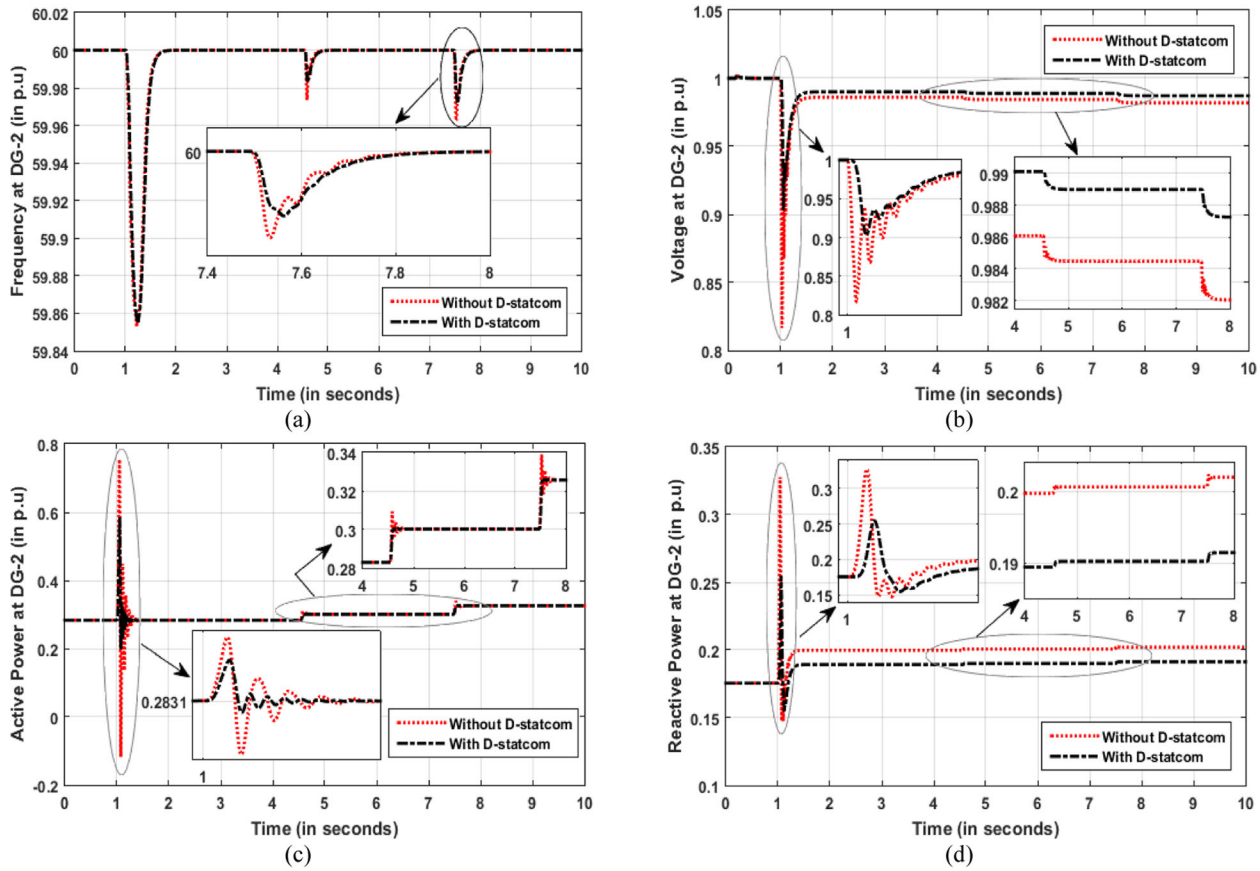

Fig. 10 Effects of D-STATCOM on the DG-2 parameters (**a**) Frequency, (**b**) Voltage, (**c**) Active power, (**d**) Reactive power

stability during the grid-forming mode of the microgrid. Further, the power-sharing scheme subsequent to load shedding strategy also operates to maintain a stiff system synchronization.

5 Result analysis

This section presents the efficacy of the proposed approach under the system undertaken. About four different cases are simulated to analyze the performance of the system. Initially, the performance of the compensating devices present in the test system is analyzed individually and subsequently the proposed load shedding approach. Case-1 highlights the power-sharing performance within the microgrid integrated only with a battery storage device under 5% of overloading. Case-2 is an extension of the first case. It integrates D-STAT COM into the system and analyses its effect on the distributed generators present in the system. Highlighting the power-sharing strategy in Case-1 and Case-2, an emphasis has been given to investigate the power-sharing and load shedding strategy together in the subsequent cases. Case-3 verifies the system stability using load

Table 1 A comparative analysis of DG power generated with and without D-STATCOM

		D-STATCOM	Peak overshoot (in p.u)	Rise time (in seconds)	Settling time (in seconds)
DG-1	P	Without	0.7326	0.006	0.192
		With	0.7184	0.044	0.148
	Q	Without	0.002998	0.015	0.191
		With	0.001992	0.024	0.132
DG-2	P	Without	0.7477	0.046	0.328
		With	0.5853	0.054	0.245
	Q	Without	0.3274	0.045	0.278
		With	0.2542	0.064	0.186

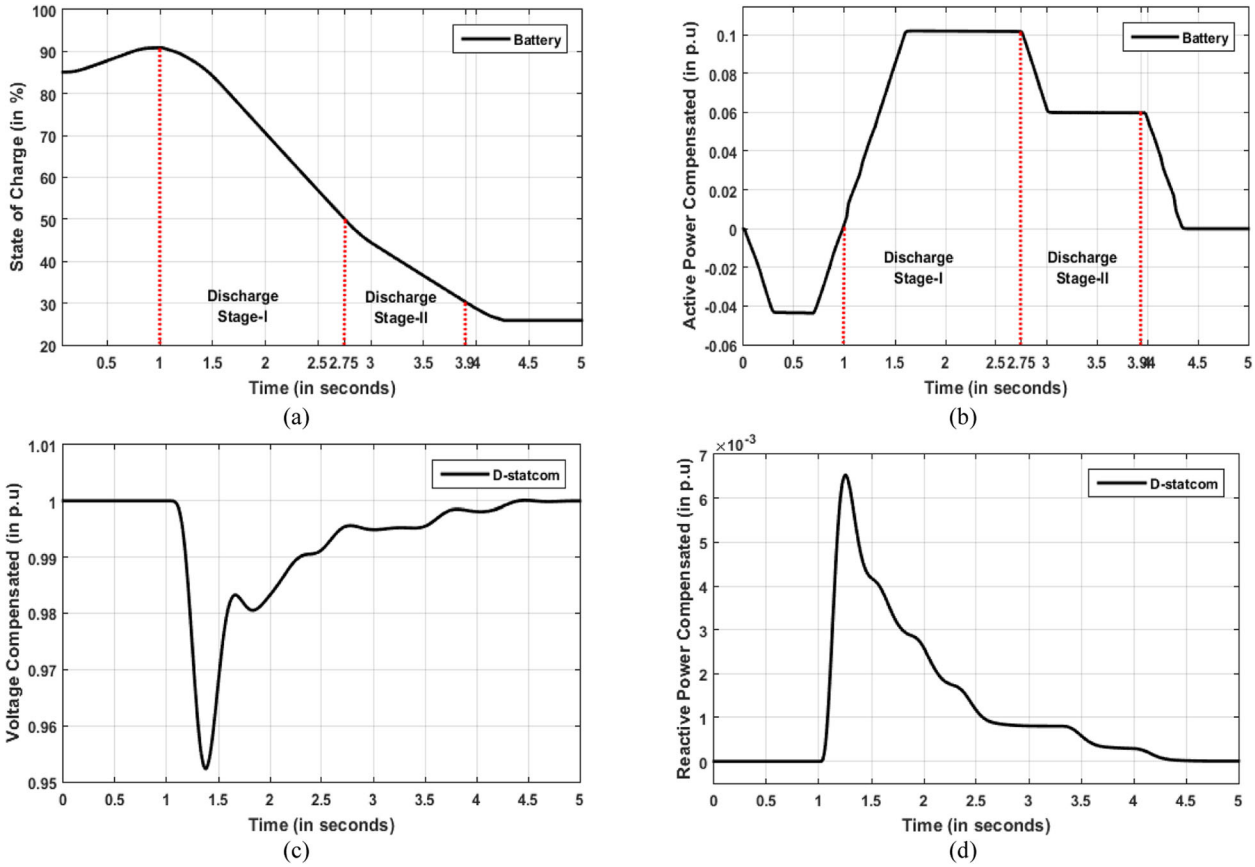

Fig. 11 Power compensated by the storage device and D-STATCOM (**a**) Battery's state of charge (**b**) Active power compensated by battery (**c**) Voltage compensated by DSTATCOM (**d**) Reactive power compensated by DSTATCOM

shedding strategy under 30% of active power and 10% of reactive power overloading condition. Further, in Case-4 the load shedding strategy is examined under a power deficit scenario, where the power generation at the DG end reduces significantly.

5.1 Case-1

The case analyses the efficient power-sharing with the operating storage system present in the microgrid. The test system is formulated with 5% of overloading with the absence of D-STATCOM. It can be analyzed from SoC and battery power, that the battery charges itself while present in a grid-connected mode. On the detection of an islanding instance (i.e., 1 s), the battery system discharges itself as shown in Fig. 7a. Thus the battery power and the synchronous generator handles the small active and the reactive power overloading of 5%.

At time 4.55 s, when the battery attains 50% of SoC, the power to be fed is reduced. On attaining the 30% of SoC at 7.49 s, the power fed by the battery is approximately zero. The active power fed by a battery based on the SoC can be studied in Fig. 7b. In the meantime, when the battery power reduces, the microgrid load demand is compensated by the synchronous generator of the microgrid. The photovoltaics do not increase its power generation as it is an MPPT based system and always supplies the maximum power in the system. The DG-2 increments the power in two steps at time 4.55 s and 7.49 s as illustrated in Fig. 7c. The reactive power fluctuations are negligible, as only the active power of the battery is compensated by the DG-2 in this case study. This negligible reactive power variation of DG-2 is presented in Fig. 7d. The increase in power generation by DG-2 is attained by reducing the DG voltage and frequency. Thus, the drop in voltage and frequency corresponding to the power increment can be analyzed from Fig. 7e and f respectively.

5.2 Case-2

Case-2 is an extension of the case-1. The system is considered with a similar overloading condition of 5% with the integrated power sources, storage device and a D-STATCOM. The power-sharing is efficient in Case-1 but the reactive power overloading is solely controlled by the synchronous generator from the instance of

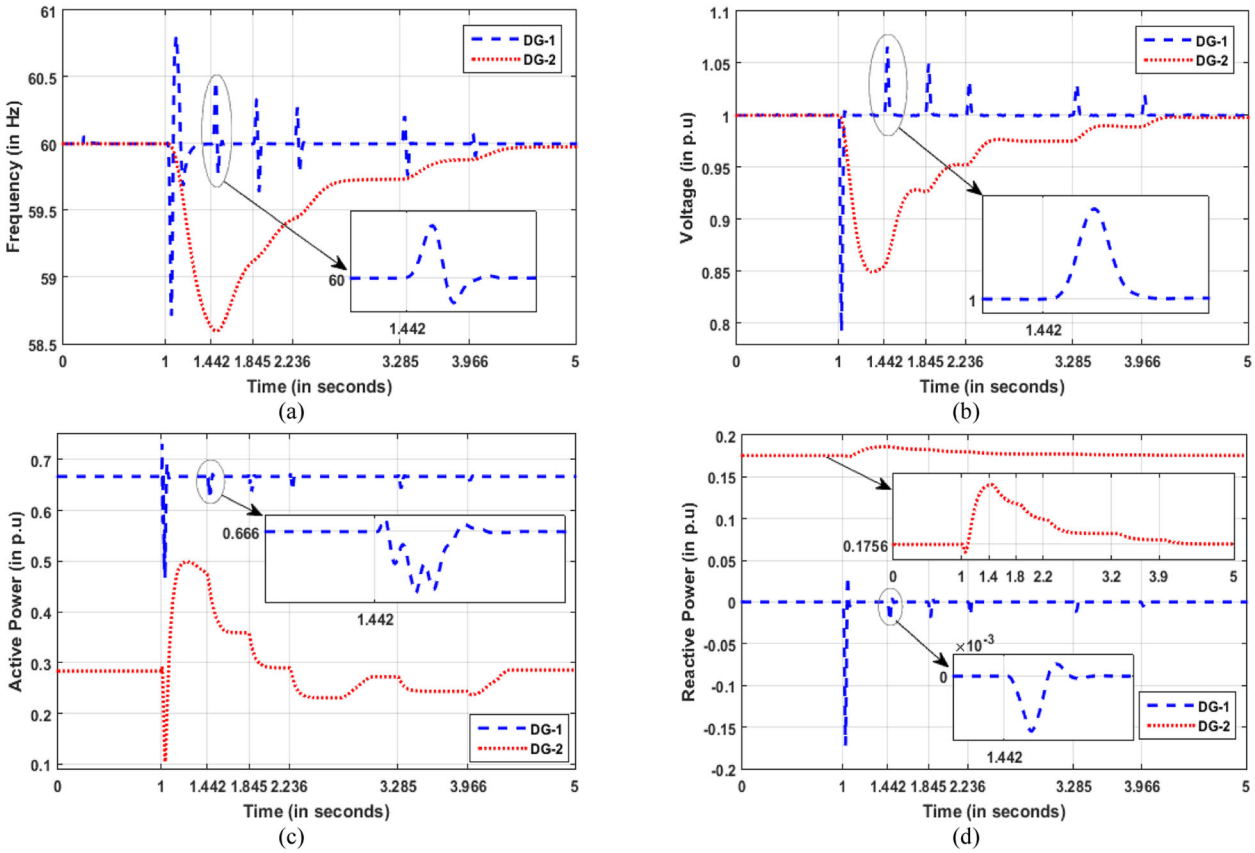

Fig. 12 DG performance during the load shedding strategy (**a**) Frequency, (**b**) Voltage, (**c**) Active power, (**d**) Reactive power

islanding. In order to support the reactive power compensation, the D-STATCOM is integrated and its effect on the system is examined in Case-2. The D-STATCOM is assumed to be triggered at the detection of an autonomous mode of operation.

The voltage control and reactive power compensated by the D-STATCOM can be examined through Fig. 8a and b respectively. It can be studied that with the reduction in battery power and an increase in synchronous generation, the D-STATCOM simultaneously increases the compensation level. Such that 60% of extra reactive power demand is fed by DG-2 and the remaining 40% of overloading is fed by the D-STATCOM. This helps in avoiding sudden stress on the synchronous generator to generate extra power beyond its generation limit.

The presence of D-STATCOM has highly enhanced the transient stability of the system and has reduced the fluctuations in the system parameters during the steady-state operation. This can be analyzed by considering a comparative study of the system responses with and without D-STATCOM. Figure 9a-d and Fig. 10a-d illustrates the effects of D-STATCOM on DG-1 and DG-2 respectively. Further, in a comparative approach, Table 1 highlights the suppression of peak overshoot and rise time

Table 2 The location and amount of the load shed

Load No.	L1	L2	L3	L4	L5	L6	L7	L8	L9	L10	L11	L12	L13	L14	L15	L16
Bus no.	1	8	7	12	7	13	9	11	10	2	5	3	4	6	6	10
Load(kW)	13.2	50	10	12.8	4.5	22.5	2.3	4.7	15	7.5	17.2	5.5	7	4.2	2.4	6.4
Priority		✓		✓		✓			✓							
Stage-I of LS			i = 2								i = 1			i = 3		
Stage-II of LS																i = 1
Stage-III of LS								i = 1								

LS Proposed load shedding strategy, *i* iteration

during transient conditions. The table also emphasizes the enhancement of the settling time in both the DGs integrated with the microgrid.

The integration of D-STATCOM suppresses the transient peak overshoot in active power by 1.938% and 21.71% in DG-1 and DG-2 respectively. It can be observed that the suppression in DG-1 is negligible, as it operates at the maximum power point. The reactive power transient fluctuation is suppressed by 21.71% and 22.35% in both DG-1 and DG-2 respectively.

5.3 Case-3

This case is stimulated at 0.86 power factor, to test the system performance under 30% of active power and 10% of reactive power overloading condition. The loads L11 to L16 are incorporated in the microgrid to simulate the overloading scenario. The case is designed such that it highlights the performance of power-sharing and load shedding strategy together. The islanding is assumed to have occurred at the time 1 s. The battery charges itself while present in grid-connected mode, and from the instance of islanding, the battery starts discharging as shown in Fig. 11a. The active power fed by the storage device is demonstrated in Fig. 11b. However, due to an extreme loading condition, the voltage and the frequency at the PCC tend to violate the threshold limit of frequency and voltage. The transient variations in voltage are compensated by the D-STAT COM as shown in Fig. 11c. The D-STATCOM also feeds an instantaneous reactive power into the system as illustrated in Fig. 11d.

The load demand in the microgrid remains too high to make the system unstable. The frequency and the voltage of the DGs tending towards the instability can be analyzed from Fig. 12a and b respectively. Thus, the violation of the system parameter's limit at PCC triggers the load shedding strategy. The loads shed by the proposed shedding strategy are calculated using (14) and the approximate similar load values with the least priority are shed as shown in Table 2.

The proposed load shedding strategy initializes the stage-I of the strategy and sheds the load in three iterations at time 1.4 s, 1.8 s, and 2.2 s. The effects of the load shedding on voltage and frequency are illustrated in Fig. 12a and b respectively. The MPP controlled DG-1 being an inertia-less power source

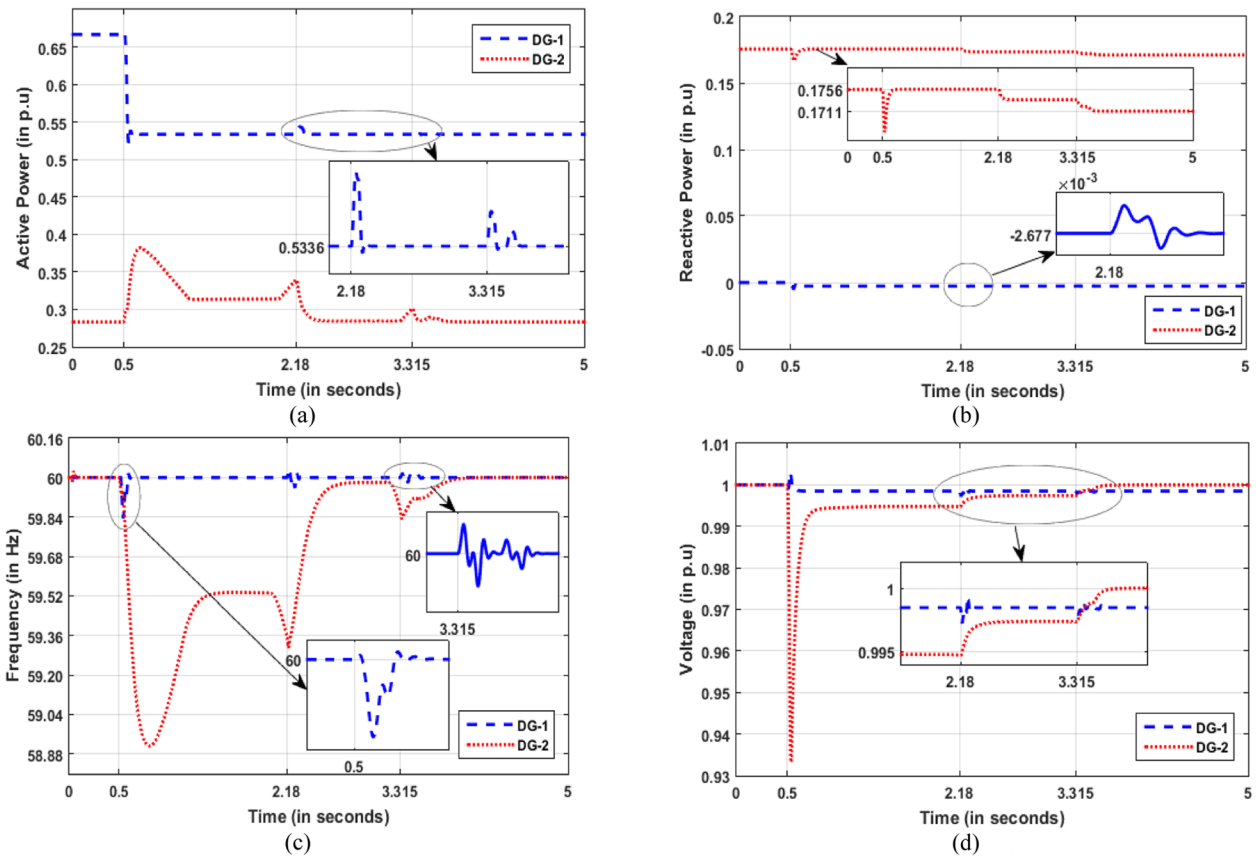

Fig. 13 System performance under reduced power generation (**a**) Frequency, (**b**) Voltage, (**c**) Active power, (**d**) Reactive power

responds with an insignificant time delay to the load shed. Whereas the DG-2 being a high inertia system shows a sluggish response and consumes a certain time to retain itself within the stability zone. The time consumed to retain the stability is compensated by the D-STATCOM present in the microgrid. The stage-I of the load shedding strategy tends the microgrid to attain the voltage and the frequency within the operating limits as shown in Fig. 12a and b.

Further, when the $\frac{df}{dt}$ condition satisfies, the stage-II of the load shedding strategy is triggered. Though the system parameters are operating within the stability limit, but to achieve the system to be operating at a standard operating point, a small load is shed at a time about 3.2 s and the stage-III of the load shedding scheme sheds another small load at 3.9 s. The variations in active and reactive power generation of DG-1 and DG-2, corresponding to the load shed can be analyzed from Fig. 12c and Fig. 12d.

5.4 Case-4

In order to examine the proposed approach under a reduced power generation, the Case-4 is simulated. The power generation by DG-1 suddenly reduces from 100 kW to 80 kW of generation. The drop of 20 kW of power from DG-1 at time 0.5 s can be analyzed in Fig. 13. The battery operates in the discharge stage-I instantly and feeds the maximum possible power of 15 kW into the system. The remaining 5 kW of power deficit is managed and fed by DG-2.

At time 2 s, the battery attains 50% of SoC and tends to operate in the discharge stage-II of the battery as shown in Fig. 14a. Thus the battery reduces the rate of discharge and feeds the power of about 9 kW as in Fig. 14b. As a result, the surplus load demand of 11 kW is to be fed by DG-2 depicted in Fig. 13a. But from Fig. 13c and d it can be observed that the increase in power deficit leads the voltage and frequency towards instability. Therefore the stage-II of the load shedding is triggered to shed the loads. So, a load is shed at 2.18 s.

This shedding of load helps the voltage and the frequency of the DGs to attain the operating point. Further, as the battery reaches 30% of its SoC, two small loads are shed by the stage-III of the load shedding strategy after 3.3 s. These shedding lead the system towards the specified operating nominal value as shown in Fig. 13 and the amount and location where the load

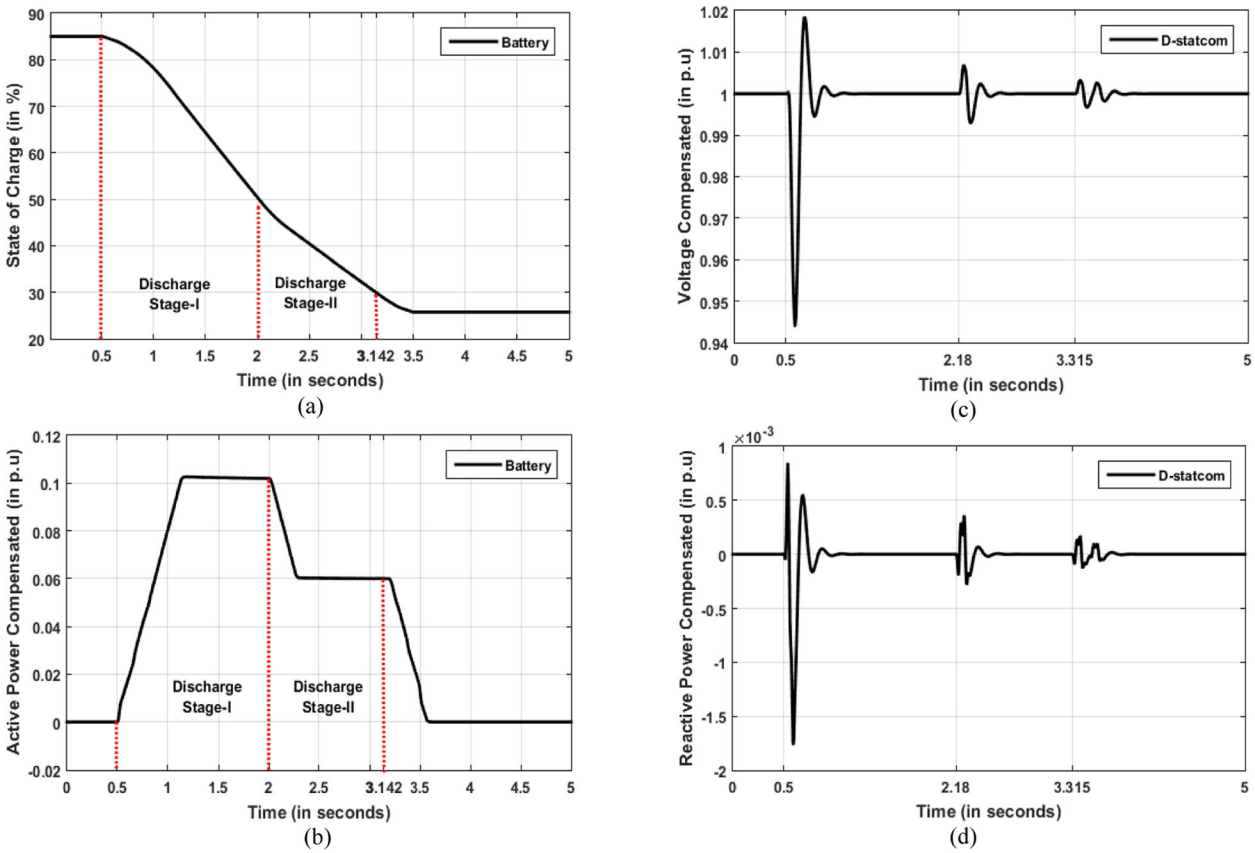

Fig. 14 Power fed by battery and D-STATCOM (**a**) Battery's state of charge (**b**) Active power compensated by battery (**c**) Voltage compensated by DSTATCOM (**d**) Reactive power compensated by DSTATCOM

Table 3 The location and amount of the load shed

Load No.	L1	L2	L3	L4	L5	L6	L7	L8	L9	L10
Bus no.	1	8	7	12	7	13	9	11	10	2
Load(kW)	13.2	50	10	12.8	4.5	22.5	2.3	4.7	15	7.5
Priority		✓		✓		✓			✓	
Stage-I of LS										
Stage-II of LS	i = 1									
Stage-III of LS					i = 1		i = 2			

LS Proposed load shedding strategy, *i* iteration

is shed in this examined case are shown in Table 3. The D-STATCOM present in this scenario only responds to suppress the transient variation occurring in the system during the reduction in power generation and load shedding as shown in Fig. 14c and d.

6 Discussion

The proposed three-stage operational strategy is tested under different scenarios to verify the efficacy. The case studies are analyzed such that the performance of ESS and D-STATCOM is significantly highlighted. The major proposal of the load shedding strategy incorporates the performance of battery storage power during the shedding process, which has been verified in the result analysis. Moreover, an efficient power-sharing within the microgrid has been analyzed to attain the system stability. The incorporation of D-STATCOM has significantly controlled the transient instances. The conventional strategies do not analyze the power-sharing while shedding loads, but the paper closely analyzes the load shedding along with an efficient power-sharing among the DGs. The most sensitive scenarios of excessive loading and decrement in power generation have been closely analyzed by the proposed strategy. In Table 4 a comparative study of the proposed strategy with the state of art has been presented to analyze the efficacy of the proposed approach.

7 Conclusion

The article aims to address the microgrid stability while operating in an autonomous mode of operation. The microgrid system undertaken integrates both inertia-less and high inertia power sources along with the storage system and the reactive power compensating device. The control strategy for each unit is elaborated in Section III of the manuscript. Each operating unit uses the P-f and Q-V power-sharing control strategy to maintain system stability. To deal with the worst-power deficit scenario, a load shedding strategy is proposed. The shedding strategy incorporates the microgrid storage system to prolong the loads for a certain time after attaining the frequency within the operational stability and limit. The D-STAT COM present in the system helps to avoid the instantaneous conflict of power-sharing between the two different types of inertial DG by compensating the voltage, and efficiently control the system stability for few cycles until the load shedding is initialized. The designed droop based load shedding strategy is only dependent on the system inertia. The strategy sheds load to control the reducing rate-of-change-of-frequency. The precise shedding process is faster compared to the conventional schemes and confirms the difference between the operating frequency and nominal frequency to be approximately zero proving its robustness to act under a wide range of operating conditions.

Table 4 A comparative study of the proposed load shedding strategy with the state-of-art

Ref	System undertaken	The efficiency of the load shedding strategy	Overall system frequency drop (in Hz)	Remarks
[17]	Microgrid (50 Hz)	98.36%	48.92	The system with synchronous and asynchronous generators
[18]	Microgrid (50 Hz)	96.82%	48.8	Implementation of an adaptive controller to maintain stability.
[21]	IEEE 14 Bus System (60 Hz)	94.50%	59.6	Load shedding without any supporting device.
[22]	Power system with interconnected power districts (50 Hz)	98.20%	49.72	Application of smart metering system for emergency shedding
[23]	Distribution system (Guadeloupean Power System) (50 Hz)	97.45%	48.5	Ultracapacitor storage to support the dynamic frequency.
[24]	Distribution system (23 bus sample system) (60 Hz)	98.34%	59.46	Super-conducting storage devices compensate the frequency variations until the governor response
[25]	Distribution System (China Steel Corporation) (60 Hz)	97.89%	58.10	Super magnetic energy storage device to enhance transient stability while shedding the loads
Proposed Approach	Modified IEEE 13-bus microgrid system (60 Hz)	99.25%	58.92	Three-stage adaptive load shedding strategy supported by battery and D-STATCOM to maintain system stability.

8 Appendix

System Rating:	
Operating frequency	60 Hz
Nominal Rated Voltage	25 kV
Base Power	150kVA
DG-1	100 kW
DG-2	50kVA (p.f = 0.86)
m_p	5e-5 Hz/W
m_q	0.1667 V/Var
T1	115 kV/ 25 kV
T2	260 V/ 25 kV
$H_{equivalent}$	312.67 s
Battery Rating:	
Battery Rating (Q)	0.226 Ah
Rated $V_{battery}$	300 V
E_0	305 V
Rated $I_{battery}$	120A
R_{int}	40mΩ
$T_{battery}$	300 V/25 kV
D-STATCOM:	
DC Capacitance	520 μF
Maximum Compensation	10kVAR
Series Reactance	4.8 μH

Abbreviations

AVR: Automated voltage regulator; BES: Battery energy storage; DG: Distributed generators; D-STATCOM: Distributed static compensator; ESS: Energy storage system; MPPT: Maximum power point tracking; PCC: Point of common coupling; PI: Proportional-integral; PV: Photovoltaic; ROD: Rate of discharge; SOC: State of charge; SPWM: Sinusoidal pulse width modulator; UFLS: Under-frequency load shedding; VSC: Voltage source converter

Acknowledgments

The authors acknowledge the financial support provided by the Council of Scientific and Industrial Research (CSIR), Government of India.

Authors' contributions

SC and PB carried out the design of the proposed study and performed the statistical analysis. PKR perceived the study, and participated in its design and coordination and helped to draft the manuscript. All authors read and approved the final manuscript.

Funding

Financial funding by Council of Scientific and Industrial Research (CSIR), Government of India.

Availability of data and materials

Data sharing not applicable to this article as no datasets were generated or analyzed during the current study.

Ethics approval and consent to participate

Not applicable.

Consent for publication

The Authors grants the Publisher the sole and exclusive license of the full copyright in the Contribution, which license the Publisher hereby accepts.

Competing interests

The authors declare that they have no competing interests.

Author details

[1]Electrical Engineering Department, Siksha 'O' Anusandhan University, Bhubaneswar 751030, India. [2]Electrical and Electronics Engineering Department, Siksha 'O' Anusandhan University, Bhubaneswar 751030, India.

Received: 25 April 2019 Accepted: 22 October 2019
Published online: 22 November 2019

References

1. Roy, N. K., Hossain, M. J., & Pota, H. R. (2011). Voltage profile improvement for distributed wind generation using D-STATCOM. In *2011 IEEE Power and Energy Society General Meeting* (pp. 1–6). IEEE; Detroit.
2. Divshali, P. H., Alimardani, A., Hosseinian, S. H., & Abedi, M. (2012). Decentralized cooperative control strategy of microsources for stabilizing autonomous VSC-based microgrids. *IEEE Transactions on Power Systems, 27*(4), 1949–1959.
3. Paquette, A. D., Reno, M. J., Harley, R. G., & Divan, D. M. (2012). Transient load sharing between inverters and synchronous generators in islanded microgrids. In *2012 IEEE Energy Conversion Congress and Exposition (ECCE)* (pp. 2735–2742). IEEE; Raleigh.
4. Majumder, R., Ghosh, A., Ledwich, G., & Zare, F. (2009). Power sharing and stability enhancement of an autonomous microgrid with inertial and non-inertial DGs with DSTATCOM. In *2009 International Conference on Power Systems* (pp. 1–6). IEEE; Kharagpur.
5. Raghami, A., Ameli, M. T., & Hamzeh, M. (2013). Primary and secondary frequency control in an autonomous microgrid supported by a load-shedding strategy. In *4th Annual International Power Electronics, Drive Systems and Technologies Conference* (pp. 282–287). IEEE; Tehran.
6. Bakar, N. N. A., Hassan, M. Y., Sulaima, M. F., Na'im Mohd Nasir, M., & Khamis, A. (2017). Microgrid and load shedding scheme during islanded mode: A review. *Renewable and Sustainable Energy Reviews, 71*, 161–169.
7. Joe, A., & Krishna, S. (2015). An underfrequency load shedding scheme with minimal knowledge of system parameters. *International Journal of Emerging Electric Power Systems, 16*(1), 33–46.
8. Rudez, U., & Mihalic, R. (2015). Predictive underfrequency load shedding scheme for islanded power systems with renewable generation. *Electric Power Systems Research, 126*, 21–28.
9. El-Zonkoly, A. (2015). Application of smart grid specifications to overcome excessive load shedding in Alexandria, Egypt. *Electric Power Systems Research, 124*, 18–32.
10. Lokay, H. E., & Burtnyk, V. (1968). Application of underfrequency relays for automatic load shedding. *IEEE Transactions on Power Apparatus and Systems, 3*, 776–783.
11. Anderson, P. M., & Mirheydar, M. (1992). An adaptive method for setting underfrequency load shedding relays. *IEEE Transactions on Power Systems, 7*(2), 647–655.
12. Delfino, B., Massucco, S., Morini, A., Scalera, P., & Silvestro, F. (2001). Implementation and comparison of different under frequency load-shedding schemes. In *2001 Power Engineering Society Summer Meeting. Conference Proceedings (Cat. No. 01CH37262)* (Vol. 1, pp. 307–312). IEEE; Vancouver.
13. Rudez, U., & Mihalic, R. (2009). Analysis of underfrequency load shedding using a frequency gradient. *IEEE Transactions on Power Delivery, 26*(2), 565–575.
14. Terzija, V. V. (2006). Adaptive underfrequency load shedding based on the magnitude of the disturbance estimation. *IEEE Transactions on Power Systems, 21*(3), 1260–1266.
15. Rudez, U., & Mihalic, R. (2011). A novel approach to underfrequency load shedding. *Electric Power Systems Research, 81*(2), 636–643.
16. Shekari, T., Aminifar, F., & Sanaye-Pasand, M. (2015). An analytical adaptive load shedding scheme against severe combinational disturbances. *IEEE Transactions on Power Systems, 31*(5), 4135–4143.
17. Karimi, M., Wall, P., Mokhlis, H., & Terzija, V. (2016). A new centralized adaptive underfrequency load shedding controller for microgrids based

on a distribution state estimator. *IEEE Transactions on Power Delivery, 32*(1), 370–380.
18. Marzband, M., Moghaddam, M. M., Akorede, M. F., & Khomeyrani, G. (2016). Adaptive load shedding scheme for frequency stability enhancement in microgrids. *Electric Power Systems Research, 140*, 78–86.
19. Ceja-Gomez, F., Qadri, S. S., & Galiana, F. D. (2012). Under-frequency load shedding via integer programming. *IEEE Transactions on Power Systems, 27*(3), 1387–1394.
20. Luan, W. P., Irving, M. R., & Daniel, J. S. (2002). Genetic algorithm for supply restoration and optimal load shedding in power system distribution networks. *IEE Proceedings-Generation, Transmission and Distribution, 149*(2), 145–151.
21. Mullen, S., & Onsongo, G. (2010). Decentralized agent-based underfrequency load shedding. *Integrated Computer-Aided Engineering, 17*(4), 321–329.
22. Chuvychin, V., & Petrichenko, R. (2013). Development of smart underfrequency load shedding system. *Journal of Electrical Engineering, 64*(2), 123–127.
23. Delille, G., Francois, B., & Malarange, G. (2012). Dynamic frequency control support by energy storage to reduce the impact of wind and solar generation on isolated power system's inertia. *IEEE Transactions on Sustainable Energy, 3*(4), 931–939.
24. Zhang, L., Liu, Y., & Crow, M. L. (2005, 2005). Coordination of UFLS and UFGC by application of D-SMES. In *IEEE Power Engineering Society General Meeting* (pp. 1064–1070). IEEE; San Francisco.
25. Hsu, C. T. (2002). Enhancement of transient stability of an industrial cogeneration system with superconducting magnetic energy storage unit. *IEEE Transactions on Energy Conversion, 17*(4), 445–452.
26. Divya, K. C., & Østergaard, J. (2009). Battery energy storage technology for power systems—An overview. *Electric Power Systems Research, 79*(4), 511–520.
27. Tan, X., Li, Q., & Wang, H. (2013). Advances and trends of energy storage technology in microgrid. *International Journal of Electrical Power & Energy Systems, 44*(1), 179–191.
28. Freitas, W., Morelato, A., Xu, W., & Sato, F. (2005). Impacts of AC generators and DSTATCOM devices on the dynamic performance of distribution systems. *IEEE Transactions on Power Delivery, 20*(2), 1493–1501.
29. Majumder, R., Ghosh, A., Ledwich, G., & Zare, F. (2009). Enhancing the stability of an autonomous microgrid using DSTATCOM. *International Journal of Emerging Electric Power Systems, 10*(5). https://doi.org/10.2202/1553-779X.2227.
30. Giroux, P., Sybille, G., Osorio, C., & Chandrachood, S. (2012). 100-kW grid-connected PV array demo detailed model. In *MathWorks File Exchange*.
31. Chandak, S., Bhowmik, P., & Rout, P. (2019). Dual-stage cascaded control to resynchronize an isolated microgrid with the utility. *IET Renewable Power Generation*. https://doi.org/10.1049/iet-rpg.2019.0062.
32. Vahedi, H., Noroozian, R., Jalilvand, A., & Gharehpetian, G. B. (2011). A new method for islanding detection of inverter-based distributed generation using DC-link voltage control. *IEEE Transactions on Power Delivery, 26*(2), 1176–1186.
33. Chandak, S., Bhowmik, P., Mishra, M., & Rout, P. K. (2018). Autonomous microgrid operation subsequent to an anti-islanding scheme. *Sustainable Cities and Society, 39*, 430–448.
34. Bhattacharya, K., & Zhong, J. (2001). Reactive power as an ancillary service. *IEEE Transactions on Power Systems, 16*(2), 294–300.
35. Canizares, C. A., Bhattacharya, K., El-Samahy, I., Haghighat, H., Pan, J., & Tang, C. (2010). Re-defining the reactive power dispatch problem in the context of competitive electricity markets. *IET Generation Transmission and Distribution, 4*(2), 162–177.
36. Majumder, R. (2013). Some aspects of stability in microgrids. *IEEE Transactions on Power Systems, 28*(3), 3243–3252.
37. Fujita, H., & Akagi, H. (2007). Voltage-regulation performance of a shunt active filter intended for installation on a power distribution system. *IEEE Transactions on Power Electronics, 22*(3), 1046–1053.
38. Benhabib, M. C., & Saadate, S. (2005). New control approach for four-wire active power filter based on the use of synchronous reference frame. *Electric Power Systems Research, 73*(3), 353–362.
39. Montero, M. I. M., Cadaval, E. R., & González, F. B. (2007). Comparison of control strategies for shunt active power filters in three-phase four-wire systems. *IEEE Transactions on Power Electronics PE, 22*(1), 229.
40. Tremblay, O., & Dessaint, L. A. (2009). Experimental validation of a battery dynamic model for EV applications. *World Electric Vehicle Journal, 3*(2), 289–298.
41. Adhikari, S., & Li, F. (2014). Coordinated Vf and PQ control of solar photovoltaic generators with MPPT and battery storage in microgrids. *IEEE Transactions on Smart Grid, 5*(3), 1270–1281.
42. Bhowmik, P., Chandak, S., & Rout, P. K. (2019). State of charge and state of power management of the hybrid energy storage system in an architecture of microgrid. *Journal of Renewable and Sustainable Energy, 11*(1), 014103.
43. Pogaku, N., Prodanovic, M., & Green, T. C. (2007). Modeling, analysis and testing of autonomous operation of an inverter-based microgrid. *IEEE Transactions on Power Electronics, 22*(2), 613–625.
44. Tabatabaee, S., Karshenas, H. R., Bakhshai, A., & Jain, P. (2011). Investigation of droop characteristics and X/R ratio on small-signal stability of autonomous microgrid. In *2011 2nd Power Electronics, Drive Systems and Technologies Conference* (pp. 223–228). IEEE; Tehran.
45. Reddy, C. P., Chakrabarti, S., & Srivastava, S. C. (2013). A sensitivity-based method for under-frequency load-shedding. *IEEE Transactions on Power Systems, 29*(2), 984–985.
46. Wang, Y., Zhou, R., & Wen, C. (1993). Robust load-frequency controller design for power systems. In IEE proceedings C (generation, transmission and distribution) (140, 1, pp. 11-16). IET Digital Library. https://doi.org/10.1049/ip-c.1993.0003.